Cavitation, Shock Waves and the Invasive Nature of Sonoelectrochemistry

Peter R. Birkin,*,† Douglas G. Offin,†,‡ Phillip F. Joseph,‡ and Timothy G. Leighton‡

School of Chemistry, University of Southampton, Southampton SO17 1BJ, United Kingdom, and Institute of Sound and Vibration Research, University of Southampton, Southampton SO17 1BJ, United Kingdom

Received: March 30, 2005; In Final Form: June 4, 2005

The invasive nature of electrodes placed into sound fields is examined. In particular, perturbations of the sound field due to the presence of the electrode support are explored. The effect of an electrode on the drive sound field (at ~23 kHz) is shown to be negligible under the conditions investigated in this paper. However, scattering of shock waves produced by cavity collapse is shown to exhibit a significant effect. To demonstrate this, multibubble sonoluminescence (MBSL) and electrochemical erosion measurements are employed. These measurements show an enhancement, due to the reflection by the solid/liquid boundary at the electrode support, of pressure pulses emitted when cavitation bubbles collapse. To first order, this effect can be accounted for by a correction factor. However, this factor requires accurate knowledge of the acoustic impedance of the interface and the electrolyte media. These are measured for two commonly employed substrates (soda glass and epoxy resin, specifically Epofix). A scattering model is developed which is able to predict the acoustic pressure as a function of position over a disk-like electrode substrate. The effects of shock wave reflection and materials employed in the electrode construction are used to clarify the interpretation of the results obtained from different sonoelectrochemical experiments. Given the widespread experimentation involving the insertion of electrodes (or other sensors) into ultrasonic fields, this work represents a significant development to aid the interpretation of the results obtained.

Introduction

Sonoelectrochemistry is the science involved with the study of cavitation processes produced by power ultrasound using electrochemical techniques. Although this field has received much attention over the past decade, the application of electrochemical techniques to the study of sonochemistry dates back to the 1930s.[1,2] In the 1960s, Nyborg *et al*. employed electrochemical techniques to study acoustic streaming processes using acoustically oscillated electrodes and arrays of electrodes.[3,4] However, in the past decade, several advances in technology have enabled sonoelectrochemistry to be exploited more extensively.[5−9] Nevertheless, it is unusual for sonoelectrochemists to consider the effects of the electrochemical technology on the sound field under investigation. It will be shown here that electrodes employed within the most commonly used sonoelectrochemical apparatus (specifically the ultrasonic horn) may have potentially significant effects on the pressure field produced in front of the electrode. As will be demonstrated in this paper, this has clear consequences for the interpretation of the experimental results.

Zang and Coury were one of the first to report the most common experimental arrangement employed for the investigation of sonoelectrochemical effects.[5] In a subsequent pioneering study, Hagan and Coury investigated mass transfer effects of an operating ultrasonic horn placed above an electrode.[9] Other investigators have adopted this experimental approach and developed important refinements to the operation and geometries employed.[7,10−13] These studies have attempted to use power ultrasound to investigate cavitation processes and the physical and chemical phenomena associated with cavitation. Birkin et al. were the first to use microelectrodes to investigate single cavitation events under a range of different experimental conditions.[14−16] The size of the microelectrodes employed in this study allowed this technique to resolve individual cavitation events and investigate the associated mass transfer effects. In an extension to this work, Birkin et al. developed an electrode with the ability to detect single erosion events associated with inertial (transient) cavitation.[17] In this and subsequent studies, an accurate control of the position (to within ±10 μm) of the microelectrode with respect to the ultrasonic horn was advocated.[18,19] In addition, consideration of the shape of the pressure−distance profile expected for such an ultrasonic source was suggested.[18]

Maisonhaute et al. have also studied cavitation by employing microelectrodes and reported multiple repetitive events under specific conditions of source-to-electrode separation.[20] Maisonhaute et al. suggested that these events were associated with a hemispherical bubble on the surface of the electrode. Clearly, these interesting differences in the nature of the results obtained within this environment require further investigation. This is the topic of this manuscript.

The sound field developed by the sound source is fundamental to the cavitation process.[18,21,22] Gas bubbles within liquids exposed to high amplitude sound waves behave in a complex and nonlinear manner. The most common way of dealing with the plethora of possible bubble behaviors is to appeal to a bimodal distinction and to describe the bubble behavior as either inertial or noninertial. Bubbles will in general pulsate (or undergo an equivalent motion if nonspherical) when subjected to an external acoustic field. The source of the "inertial/noninertial" terminology comes from the physics of the collapse phase of this pulsation: if the inertial forces dominate during

* Corresponding author. E-mail: prb2@soton.ac.uk.
† School of Chemistry.
‡ Institute of Sound and Vibration Research.

10.1021/jp051619w CCC: $30.25
Published on Web 08/11/2005

the collapse (i.e., the inertia of the converging liquid), then the collapse is "inertial". If instead the pressure forces dominate during the collapse (these act through the stiffness of the gas within the bubble), then the collapse is termed "noninertial". While this distinction accurately encapsulates the physics, sonochemists are more familiar with the phenomenological distinctions between the two: in multibubble systems (as distinct from single bubble[23] experiments), it is inertial cavitation which is associated with most of the effects in which they are interested. These effects include the generation of radical species,[24−27] unusual chemistry (high temperatures and pressures), the emission of light pulses (termed multibubble sonoluminescence,[22] MBSL), and the erosion of surfaces.[17,18]

In parameter space, the distinction between inertial and noninertial cavitation is a threshold, primarily defined by the acoustic pressure amplitude, the acoustic frequency, and the size of the bubble before the sound field was imposed (it also depends on other parameters, such as surface tension and viscosity, but these are rarely considered as control variables, because the common scenario is to control the amplitude and frequency of the sound field, rather than adjust the liquid properties). Note that if there is no pre-existing bubble, then the relevant threshold is one relating to the nucleation of that bubble. In this experiment, all the data were taken in aerated liquids after several seconds of continuous insonification. Hence, at all points where data are taken in this paper, there has been a very great number of pre-existing bubbles present. Therefore, the threshold under consideration in his paper is the inertial cavitation threshold, and not the nucleation threshold. If the experiment were instead using short microsecond bursts of ultrasound in a degassed sample, then the nucleation threshold may have been more important, but that was not the case here. In an aerated aqueous solution in the low kilohertz range (20−40 kHz), this inertial cavitation threshold pressure for the generation of inertial cavitation is ∼1 bar (zero-to-peak).[28]

Understanding the behavior of gas bubbles within a liquid is key to the interpretation of any sonoelectrochemical experimental data obtained. However, little attention has been paid to the effect of the electrode itself on the pressure field developed by the operating ultrasonic horn. While one assertion is that the electrode has a negligible effect on the sound field,[29] we present here clear experimental and theoretical evidence to suggest that the electrode is indeed invasive. The presence of the electrode therefore alters the pressure field which can change the behavior of the bubbles present in the liquid and hence the interpretation of the experimental results. These findings indicate that the apparent differences in experimental results reported in the literature could be due, in part, to scattering by the electrode support rather than a direct experimental or interpretation error.

Experimental Section

Apparatus and Methods. The apparatus required for the sonoelectrochemical measurements has been reported previously.[15,18] Epoxy-bodied Pb/Pt dual microelectrodes were constructed by sealing lead (125 μm diameter) and insulated platinum (50 μm) wire in Epofix epoxy resin, as described previously.[18,19] For the glass-bodied electrode, the following method was used. Two platinum wires (125 and 50 μm diameters) were sealed in glass by the scientific glass blowing service at the University of Southampton in such a way that they remained electronically isolated from each other, but within ∼300 μm. The 125 μm wire was etched in the sonoelectrochemical cell using a two-electrode arrangement with a vitreous carbon rod acting as the counter electrode. The applied potential was switched between +6 and −6 V at a frequency of 25 Hz (0.02 s pulses). The etching solution consisted of 60% saturated $CaCl_2$, 36% H_2O, and 4% concentrated HCl (by volume). During etching, the solution was cavitated at a horn-to-electrode distance of 5 mm in order to remove reaction products from the cavity. The progress of the etching was monitored using an optical stereomicroscope, and it was stopped when the depth of the cavity was approximately 100 μm. Following the etching process, the electrode was thoroughly rinsed and lead was deposited in the cavity potentiostatically using a three-electrode setup. A ring of platinum mesh acted as the counter electrode, and a saturated calomel electrode (SCE) was used as the reference. The ring was positioned around the tip of the glass electrode to create a uniform current density profile. The deposition solution consisted of 0.3 mol dm^{-3} $PbCO_3$ in 2 mol dm^{-3} CH_3SO_3H. A cyclic voltammogram of the recessed platinum electrode in a lead deposition solution (and a side view image of the tip of the electrode) is shown in Figure 1. The onset of lead deposition is marked by the sharp increase in cathodic current at ∼ −0.42 V vs SCE. On the positive scan, there is a large peak due to stripping of the deposited lead. To produce the desired Pb/Pt dual electrode (to match the epoxy system, see the results section), it was necessary to deposit electrochemically Pb into the recess. A current−time trace for the deposition of lead into the recess is shown in Figure 2. The electrode was initially held at a potential of +0.5 V vs SCE. The potential was then stepped to −0.5 V vs SCE, which is in the potential region where lead deposition occurs. To accelerate the deposition process, the solution was cavitated using an ultrasonic horn at a horn-to-electrode distance of 5 mm in order to promote mass transfer. The enhancement in mass transfer of Pb^{2+} to the electrode surface is indicated in Figure 2. At this point, the potential was adjusted such that the current density was ∼200 mA cm^{-2}. Over the first 400 s, the current increases gradually as the cavity fills with lead. There is then a clear transition between 400 and 500 s after which the current increase is much faster. The total charge passed up to this point was ∼15 mC, which equates to 1.42×10^6 μm^3 of lead or, assuming a diameter of 125 μm and 100% efficiency, a depth of 115 μm. This is in good agreement with the image of the recessed electrode shown in Figure 1 and indicates that the rapidly increasing current seen after 500 s is the result of lead deposition outside of the cavity. This change in behavior is a good indicator

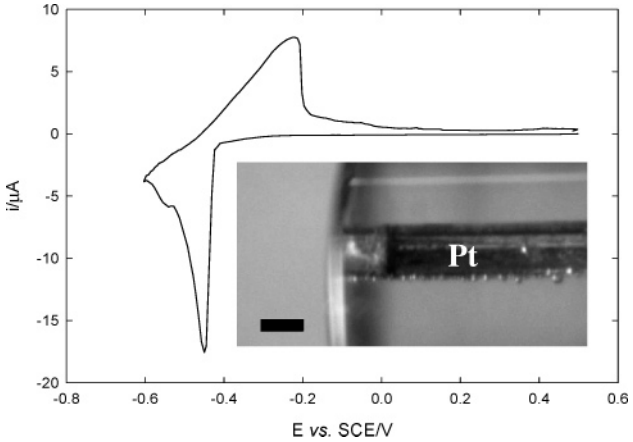

Figure 1. Cyclic voltammogram of a recessed platinum electrode (125 μm diameter) in a solution of 0.3 mol dm^{-3} $PbCO_3$ in 2 mol dm^{-3} CH_3SO_3H. The sweep rate was 20 mV s^{-1} and the temperature was 25 °C. The inset shows an image of the recess formed in the tip of the etched electrode. The scale bar represents 100 μm.

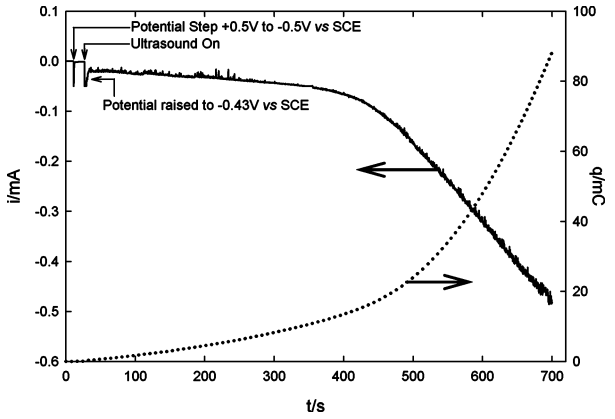

Figure 2. Plot showing the current (—) and charge (····) as a function of time during the deposition of lead at the recessed electrode. The deposition solution is described in Figure 1.

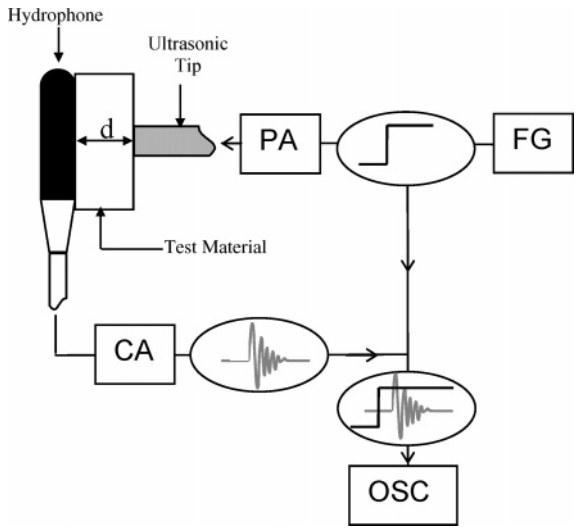

Figure 3. Experimental setup for the measurement of the speed of sound. FG = function generator, PA = power amplifier, CA = charge amplifier, OSC = oscilloscope.

as to when the deposition is complete. Subsequent polishing results in a lead/platinum dual electrode, which was then used to locate the inertial cavitation threshold as described in the results section. All experiments were performed at 25 °C under aerobic conditions.

The speed of sound was measured using a Bruel & Kjaer 8103 hydrophone, 2635 charge amplifier, and the ultrasonic transducer, via a function generator and power amplifier. For the solid samples, the experimental setup is shown in Figure 3. The function generator sends a pulse to the transducer. This signal is also used to trigger an oscilloscope. The hydrophone detects the pulse, which is recorded by the oscilloscope via the charge amplifier. The delay between the trigger and detection of the pulse is proportional to the speed of sound in the test material. Disks of various thicknesses, *d*, were used in order to determine the linear relationship between delay time and *d*, from which the speed of sound could be deduced (a technique which is far more accurate than use of the absolute value of *d*, with its uncertainties and end effects). For the electrolyte, the same technique was used except the hydrophone was placed in the solution and the horn-to-hydrophone distance was controlled by a micrometer and stage. The results of this analysis on the materials employed are reported in Table 1.

Imaging Experiments. A Starlite Xpress HX5BC cooled 16-bit CCD camera was used to image luminescence produced by the cavitation induced by the ultrasonic horn. The exact experimental conditions are given in the appropriate figure legends.

TABLE 1: Measured Physical Properties of the Materials Used Together with the Associated Reflection Coefficient

material	density (kg m^{-3})	speed of sound (m s^{-1})	*R*
electrolyte	1110 ± 20	1610 ± 20	
Epofix epoxy	1120 ± 70	3100 ± 350	0.32 ± 0.09
glass	2300 ± 100	4000 ± 500	0.67 ± 0.13

Chemicals. All solutions were made up using water from an USF Elga Purelab Option E10 water purification system. Water purified in this manner had a conductivity of below 0.1 μS cm^{-1} and a low organic content (TOC < 30 ppb). Na_2SO_4 (BDH, AnalaR), $K_4Fe(CN)_6$ (Aldrich, 99%), $CaCl_2$ (Aldrich, 99.99%), HCl (BDH, Aristar), $PbCO_3$ (BDH, GPR), CH_3SO_3H (Aldrich, 99.5%), and Epofix resin (Struers) were used as received. Electrode materials were obtained from Goodfellow.

Results and Discussion

MBSL Studies. A previous study indicated that the threshold for inertial cavitation, measured by imaging the spatial characteristics of MBSL produced by an operating ultrasonic horn, was lower than the theoretical value.[18] This suggested that a secondary effect, attributed to shock wave generation due to cavity cluster collapse, affected the behavior of bubbles close to the tip of an operating ultrasonic horn. This observation poses a further question as to the effect of an electrode on the sound field within this environment.

The invasive nature of electrodes placed within a sound field can be demonstrated by analysis of MBSL images in the absence and presence of an electrode. Figure 4 shows the effect of an electrode on the spatial distribution of the light emission from an operating ultrasonic horn. Light emission in the absence of an electrode body can be seen to be concentrated at the tip of the operating ultrasonic horn. This is in agreement with the predictions of the spatial variation of pressure produced by such sound sources. Above the inertial cavitation threshold, luminescence is observed in a small region close to the tip of the ultrasonic horn. However, if an electrode is immersed into this environment, then the presence of the electrode causes increased pressure directly in front of the electrode body. This is clearly demonstrated in Figure 4c and d. These results show that the luminescence has been extended to greater distances by the presence of the solid electrode body. Figure 4e shows an image constructed by subtracting image b from image d. The extended light emission due to the presence of the electrode is clearly apparent.

To understand this effect, it is necessary to describe briefly the scattering of sound from a disk-like object (e.g., the electrode) as a function of the electrode size, the sound frequency, and the materials employed in the experiment. In this paper, the influence of the electrode on the incident sound field is estimated by computing the total (incident plus scattered) pressure over its face. The bulk of the electrode (e.g., the insulating support) will be approximated as a disk-shaped object. The estimation of scattered pressure is based on linear acoustic theory, although it is recognized that high amplitude acoustic fields may exhibit some degree of nonlinear behavior. The linear assumption is supported by calculating the errors associated with not using a nonlinear theory.[30] For example, at the drive frequency (23 kHz) and assuming a 10 bar amplitude, the pressure associated with the second harmonic is ~0.03% of the fundamental, while, at 1 MHz, the pressure associated with the

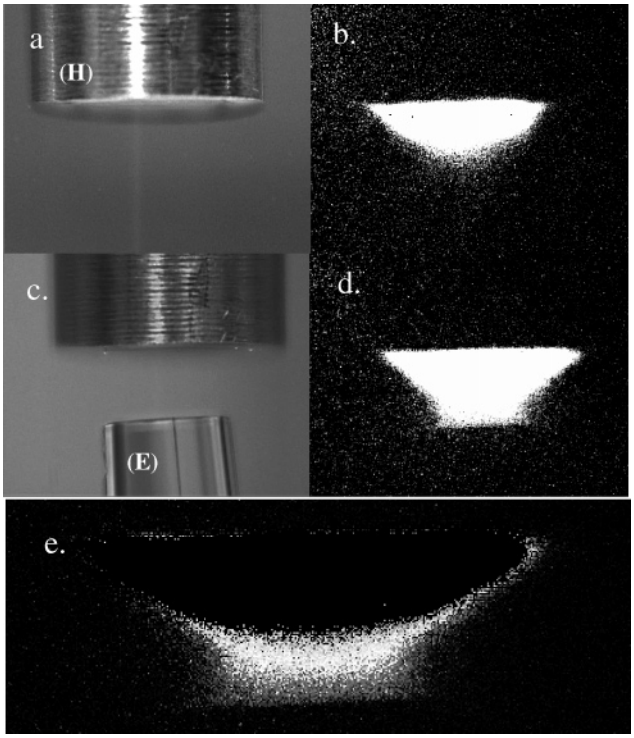

Figure 4. Images of the ultrasonic horn and electrode taken with a cooled CCD camera. Frames a and c were taken under normal daylight conditions, while frames b and d were taken in a dark room. Frame a shows the ultrasonic horn (labeled H) on its own and frame b the corresponding light emission (exposure time 10 min) in the presence of continuous ultrasonic irradiation (22.85 kHz, 56 W cm^{-2}). Frame c shows the ultrasonic horn with a glass mounted electrode (labeled E) (25 μm stainless steel) and frame d the corresponding light emission (exposure time 10 min) in the presence of continuous ultrasonic irradiation (22.85 kHz, 56 W cm^{-2}). The solution contained 0.75 mol dm^{-3} Na_2SO_4. The experiment was performed under ambient conditions (25 °C, aerobic solutions). The horn diameter was 3 mm. Image e shows a subtraction of frame b from frame d.

second harmonic is ~1.4% of the fundamental. In both cases, a propagation distance of 4 mm is assumed (corresponding to twice the horn-to-electrode distance at a typical inertial threshold determined using the electrochemical detection method). The incident pressure variation in the absence of the electrode is assumed to be a single-frequency plane wave normally incident upon the disk with pressure amplitude p_i. For generality, we assume that the disk is made from a non-rigid material, such that the particle velocity of the incident wave, u_i, and the scattered particle velocity, u_s, immediately adjacent to the disk, are related by a normal-incidence pressure plane wave reflection coefficient, R. Here, $R = (\rho_2 c_2 - \rho_1 c_1)/(\rho_2 c_2 + \rho_1 c_1)$ for waves in medium 1 (of sound speed c_1 and density ρ_1) reflecting from the interface with medium 2 (of sound speed c_2 and density ρ_2). Figure 5 presents that variation of R as a function of ρ_2 and c_2, corresponding to the material used in the experiments. Note that the literature values for the relevant materials chosen are shown in Figure 5.[31−33] Exact values for the materials used in this study are accurately determined (see Experimental section and Table 1). This leads to the following relationship between the scattered, u_s, and incident, u_i, particle velocities at the electrode surface:

$$u_s = -Ru_i \tag{1}$$

The plane wave assumption made here allows the particle velocity of the incident sound field (and hence u_s though eq 1)

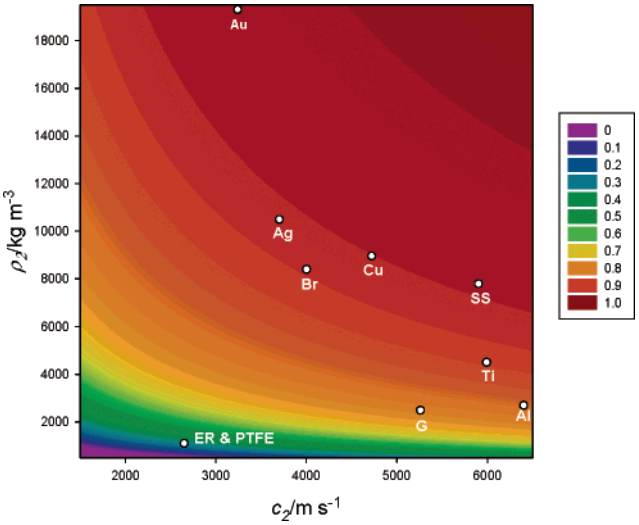

Figure 5. Plot showing the pressure reflection coefficient (see color scale), R, as a function of electrode support material and assuming immersion in water of sound speed 1480 m s^{-1} and density 990 kg m^{-3}. This calculation assumes a fluid/fluid model. A number of different materials are included on the plot. ER & PTFE represent epoxy resin and Teflon, respectively, G represents glass, SS, stainless steel, and Br, brass. All other symbols refer to the pure elements. The data were obtained from a number of reference sources.[31−33]

to be related to its acoustic pressure, p_i, through

$$u_i = p_i/\rho_1 c_1 \tag{2}$$

Equations 1 and 2 specify the fluctuating fluid velocity distribution over the disk electrode surface in terms of the pressure amplitude, p_i, of the incident wave. A compete analysis of this problem is presented in the Appendix. It is shown that the pressure variation over the face of the electrode (of radius a) may be written in the form

$$p(r,t) = p_i(t) + p_s(r,t) = p_i e^{j\omega t}[1 + R(1 - H(ka,\bar{r}))] \tag{3}$$

where $H(ka,\bar{r})$ is a nondimensional scattering function, which is completely defined by the nondimensional parameters of ka and $\bar{r} = r/a$. It is shown that, under certain conditions, $H = -1$, which for a rigid electrode $R = 1$ in eq 3, predicts that the maximum pressure at the face of the electrode is $p(r,t) = 3p_i(t)$. Of interest in this paper is the pressure averaged over the surface of the electrode, $\langle p \rangle = S^{-1}\int_S p(\mathbf{x})\, dS(\mathbf{x})$. A similar analysis is involved in the calculation of the radiation impedance of a baffled circular piston. This was first performed by Lord Rayleigh in 1896, whose solution is expressed in terms of tabulated functions. As demonstrated in the Appendix, following an identical approach, $\langle p \rangle$ may be written in the form

$$\langle p \rangle = p_i e^{j\omega t}\left[1 + R\left(1 - \frac{2J_1(2ka)}{2ka} + j\frac{2K_1(2ka)}{2ka}\right)\right] \tag{4}$$

where J_1 is the Bessel function of the first kind (order 1), K_1 is the Struve function (order 1), k is the acoustic wavenumber ($2\pi f/c_1$, where f is the frequency of sound), and a is the radius of the disk-shaped electrode support. Note that the radial pressure variation and the average pressure are completely defined by the nondimensional frequency, ka, also known as the Helmholtz number. The Helmholtz number may also be interpreted as a nondimensional measure of the disk radius, that is, $ka = 2\pi a/\lambda$. Figure 6 shows a plot of eq 4 versus ka for a variety of R values.

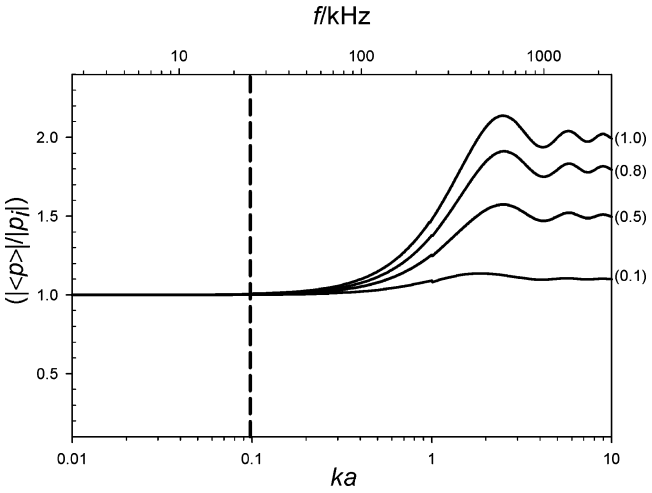

Figure 6. Plot showing the surface averaged pressure at a disk as a function of *ka* or the drive frequency, *f*, assuming $a = 1$ mm. The solid lines represent the analytical model (eq 4). The values of *R* employed are shown in parentheses beside the appropriate plot. The vertical dashed line shows the value of *ka* for the experiment employed here considering a driving frequency of 23 kHz.

Considering the drive signal (~23 kHz) and electrode support radius (~1 mm) employed here, a value of $ka = 0.098$ is obtained. First, consider the case where the boundary between the electrode support and the electrolyte can be assumed to be rigid (e.g., $R = 1$). Under these circumstances, the scattering of the incident driving sound field by the electrode ($ka = 0.098$, see Figure 6) is predicted to be negligible. However, for higher *ka* values (e.g., $ka > 0.5$ corresponding to high frequency components produced by the cavitation process), then the scattered pressure becomes significant when compared to the pressure amplitude of the incident sound waves. Hence, for frequencies of sound significantly greater than a drive frequency of 23 kHz (e.g., see the high frequency nature[34] of the shock waves produced by cavitation in Figure 4 of ref 18 and later discussion), the disk electrode support scatters strongly the incident acoustic field. This implies that shock waves (emitted by cavitation) will be reflected from the solid/liquid boundary of the electrode, which then modifies the sound field to be measured. As a result, a shock wave with a magnitude of 0.9 bar will become 1.8 bar at the surface of the electrode. This will have important ramifications in relation to the fate of bubbles within such a sound field. Bubbles which would be classified as noninertial (in the absence of the electrode) can become inertial due to this extra pressure as a result of the scattering produced by the electrode. This effect is apparent in the MBSL images obtained and shown in Figure 4. For example, the MBSL image, shown in Figure 4d, indicates luminescence at further distances compared to the situation in the absence of the electrode (see Figure 4b and e). This is supporting experimental evidence for this scattering effect. It should be noted that it is the absolute value of the pressure imposed by the acoustic field (e.g., the drive frequency, the shocks, and the scattered contribution of each) on the bubbles that is the important factor in this argument, taking into account the rapid response time of small bubbles and the threshold nature of the inertial/noninertial distinction in bubble behavior.

Second, consider the case where the boundary between the electrode support and the electrolyte cannot be assumed to be rigid (e.g., $R < 1$). This is the case for many materials that may be employed in the construction of electrodes for sono-electrochemical experiments. Under these conditions, it is possible to calculate the scattered pressure using eq 4 (see Figure 6) as a function of the electrode support dimensions, the materials used, and the frequency of sound employed. In the high frequency limit (e.g., $ka > 2$) to first order, the scattered average pressure over the surface of the electrode tends to a value of $\langle p \rangle = (1 + R)p_i$ (rather than $\langle p \rangle = 2p_i$ for the rigid model). It should be noted that this model is based on the assumption that the incident sound field is a plane wave impinging on the electrode at normal incidence. Waves arriving at the electrode at oblique incidence will generate shear waves in the electrode, leading to a value of *R* that differs from that predicted by the fluid/fluid model assumed here.[35] Last, if a periodic nonlinear waveform is incident on the face of the electrode with a period equal to that of the incident signal, a Fourier series decomposition of this waveform gives the amplitudes of its various harmonic component frequencies. The scattering of each of these harmonic components by the electrode may be treated separately. However, as explained previously, it is envisaged that the pressure amplitude of the harmonic frequencies of order two and higher may be neglected for drive pressure amplitudes of up to at least 10 bar.

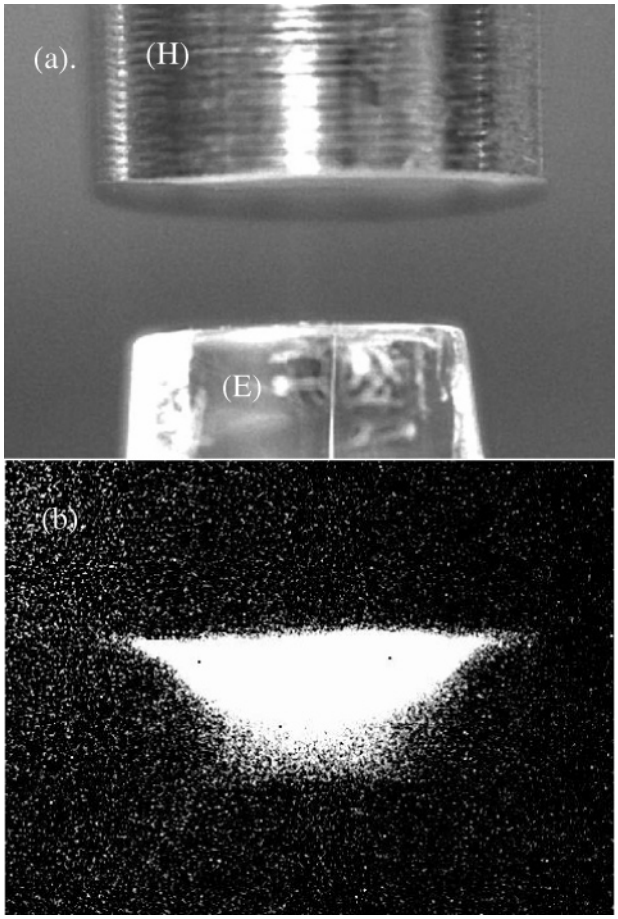

Figure 7. Images of ultrasonic horn and epoxy electrode taken with a cooled CCD camera. Frame a was taken under normal daylight conditions, while frame b was taken in a dark room. Frame a shows the ultrasonic horn (labeled H) and epoxy-bodied electrode (labeled E). Frame b shows the corresponding light emission (exposure time 10 min) in the presence of continuous ultrasonic irradiation (22.85 kHz, 56 W cm^{-2}). The solution contained 0.75 mol dm^{-3} Na_2SO_4. The experiment was performed under ambient conditions (25 °C, aerobic solutions). The horn diameter was 3 mm.

MBSL imaging of the operating ultrasonic horn in the presence of an epoxy bodied electrode (as opposed to glass) provides supporting experimental evidence for this pressure reflection effect. Figure 7b shows a MBSL image obtained in the presence of an epoxy electrode. Again, extended lumines-

cence is observed in comparison to the images obtained without the electrode (see Figure 4b). However, the extension of luminescence is not as striking as that shown for the glass electrode support (see Figure 4d). This can be explained by considering the acoustic impedance of epoxy resin and glass with respect to the electrolyte. This will, in turn, affect the plane wave normal reflection coefficient, R (see Table 1). This analysis shows that the glass electrode scatters considerably more when compared to the epoxy electrode ($R = 0.32$ vs 0.67 for epoxy vs glass, respectively). Hence, the difference in the MBSL images for the glass and epoxy electrodes can be explained by their respective reflection coefficients. As an example, a 5 MHz wave of amplitude 0.36 MPa in the absence of an electrode will be reflected by the epoxy substrate to 0.47 MPa (below the inertial threshold; see ref 36), while for the glass substrate, the scattered pressure reaches a value of 0.6 MPa. Depending on the frequency, the ability to increase the local pressure amplitude may be enough to cause an originally noninertial bubble to become inertial and hence emit light. This difference is due to the differing R values of the two materials and is supported by MBSL imaging of the two systems.

However, the insertion of a solid body into a liquid can in principle affect the cavitation field other than by its effect on the pressure field. In addition to perturbing the acoustic field, their physical presence can affect the cavitation, for example, via the distribution of cavitation nuclei. The effect goes beyond the simplistic assertion that volumes from which the liquid has been displaced, to be replaced by nonporous solid, cannot cavitate. The interfaces between solid and liquid are well-known for their ability to nucleate cavitation.[36] When ultrasonic fields are passed through a liquid, as in this paper, it is no simple matter to assign responsibility for an observed change in cavitation to the perturbations of the pressure field or to the availability of nucleation. However, in 1850, Berthelot undertook static tests of liquid samples, in which the effect of the pressure field is removed, leaving only the issue of nucleation.[37] The sample was heated in a closed glass tube which was almost filled with liquid, with the remainder of the volume being gas. On heating, the liquid expanded more than the glass, forcing the gas into the liquid, so that the latter filled the vessel. On cooling, the liquid adhered to the glass: since the liquid was thus restrained from contraction, tension was generated within it. The tension increased as the liquid cooled, until cavitation occurred. With this technique, Berthelot measured the "tensile strength" of his water sample to be around 50 bar. However, this value did not represent the tensile strength of the water *per se*. Rather, it reflects the invasive nature of the solid/liquid interface with respect to cavitation nucleation. This is because the crucial observation for our purposes was that the cavitation in Berthelot's experiments initiated at the walls of the tube, rather than in the body of the liquid. It was therefore the forces of adhesion between glass and liquid that were overcome, not the cohesion between the liquid molecules. This demonstrates an important point: it is not the properties of the liquid *per se* that determine the maximum tension a liquid can sustain but often the other bodies present within the liquid sample.[38]

Berthelot's tests were static and demonstrated the invasiveness of the insertion of a solid with respect to nucleation. They do not contain information on the relative magnitude of this effect, compared to the perturbation by the solid of the pressure field. However, Figure 4e shows that the majority of the additional sonoluminescence which results from the insertion of the solid occurs on the perimeter of the boundary which divided, prior to the insertion of the solid, that region of the liquid in which inertial cavitation occurred from that region where it did not occur. This boundary is defined by the local values of the *acoustic pressure* in the liquid, which in the free field reduces in amplitude as one moves further away from the transducer. The theory predicts that acoustic reflection at the surface of the solid will increase the pressures in this region, and this will have exactly the effect of allowing that boundary to extend further from the source than it otherwise did. The majority of the additional luminescence is not at the interface of the solid/liquid boundary. That is not to say that the effect on nucleation is always expected to be less than that on the pressure field. However, the evidence from Figure 4 is that this is the case here. In addition, it should also be noted that the surface of the electrode is highly polished (to 0.3 μm) which is likely to suppress the effect of surface nucleation. Last, Figure 4 shows that the luminescence is located above the upper face of the electrode. This is to be expected considering a scattering model as proposed here. However, an explanation relying on surface nucleation would suggest that luminescence, particularly considering that the sides of the electrode are not polished, would also occur down the sides of the electrode body. This is not observed, providing further experimental evidence for the scattering model over a model based on surface nucleation.

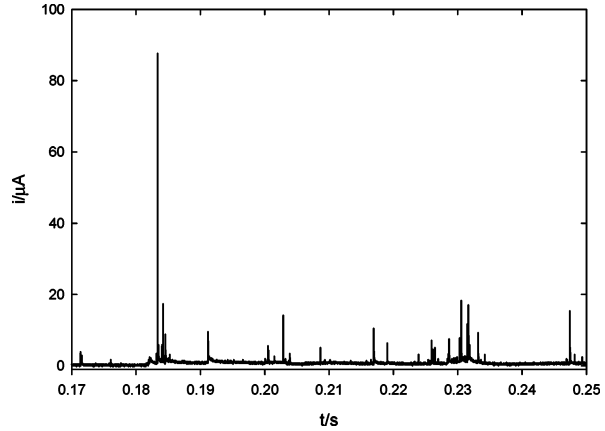

Figure 8. Plot showing a current−time trace recorded for a passivated lead electrode (125 μm diameter) sealed in epoxy resin in the presence of continuous ultrasonic irradiation (22.85 kHz, 56 W cm^{-2}). The electrode-to-tip separation was 0.9 mm, and the potential was held at +0.8 V vs SCE. The sampling rate was 125 kHz.

Electrochemical Evidence. The above discussion has shown that the frequency characteristics of the sound field, the materials used in the construction of the electrode, the electrolyte properties, and the electrode size are important in determining the scattering effect of the electrode with respect to inertial cavitation within experiments. Thus far, this effect has been supported by experimental evidence gained through MBSL imaging. While this clearly shows the effect of the electrode on the spatial distribution of inertial cavitation events (inferred from luminescent bubbles), it is a somewhat qualitative technique. In contrast, an electrochemical technique has recently been described which allows the location of the inertial cavitation threshold to be determined in terms of the axial distance from the tip of the ultrasonic horn.[18] This method uses the reoxidation of a passivated lead electrode[17] following erosive processes as a sensor for individual inertial cavitation events.

Figure 8 shows a typical example of a current−time trace recorded at a horn-to-electrode distance of 0.9 mm for an epoxy mounted electrode. By monitoring the number of erosion events as a function of axial distance from the tip of the ultrasonic horn, a threshold distance can be established. This distance demarcates locations in the solution where inertial cavitation is

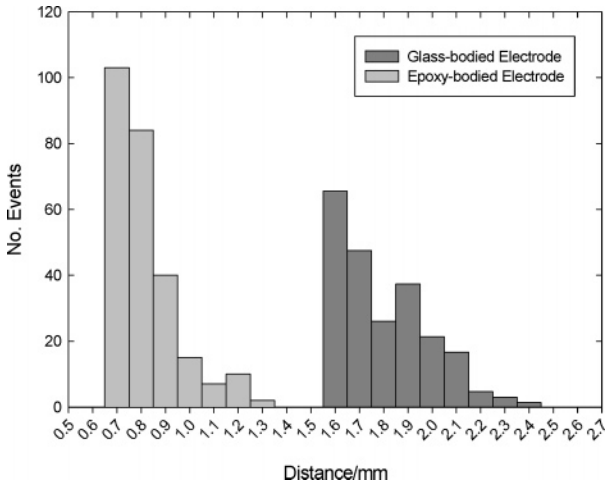

Figure 9. Plot showing the average number of erosion events detected in 0.4 s as a function of the axial distance between the electrode and the tip of the ultrasonic horn for glass- and epoxy-bodied lead electrodes. Note the experiment was terminated when the event count exceeded ~150 counts/s (i.e. at distances <1.6 mm for glass and <0.7 mm for epoxy). This was to preserve the lead electrode which can become extremely recessed if exposed to continuous inertial cavitation. However, the number of erosion events detected is expected to increase as the distance is reduced further.

present from those where it is not. The acoustic pressure amplitude at this location is deemed to be the threshold pressure for inertial cavitation. However, as discussed above, for a given location in the sonoelectrochemical cell, the pressure at the surface of an electrode will depend on the physical properties of the materials used in its construction. In accord with this, the location of the threshold for erosion events will be different for different electrode materials (see Figure 5 and Table 1). To test this and support the MBSL data, it was necessary to develop a technique for determining the acoustic impedance of the materials used in this work (see the Experimental Section and Table 1) and for manufacturing a lead electrode sealed in an alternative material to epoxy resin. In this case, glass was chosen. However, sealing lead into glass is extremely difficult, and thus, a new method was developed. This method enabled the deposition of lead into the recess formed following the etching of a platinum electrode (see the Experimental Section) to be achieved. Hence, a dual Pb/Pt electrode was manufactured and the boundary between inertial and noninertial events (as detected through electrochemical erosion[18]) determined for this new electrode.

Figure 9 shows the number of erosion events recorded in 0.4 s as a function of the distance between the electrode and the horn emitter for electrodes constructed of different support materials. The number of peaks was counted using a simple computer program, which defines a peak as any point that is greater than the previous (and a set trigger value) and is followed by four decreasing data points. In both cases, the trigger current was set at 5 μA. Clearly, it is possible to detect erosive events and hence inertial cavitation at greater distances with the glass-bodied electrode than the epoxy-bodied electrode. The thresholds for the onset of erosion were found to be 1.3 ± 0.2 and 2.3 ± 0.2 mm for epoxy and glass electrode supports, respectively.

Again, this can be readily explained by considering the pressure profile of the sound field generated by the ultrasonic horn, the generation of shock waves (through a concerted cavity cluster collapse model[39,40]), and the material properties of the electrodes employed. Under the sonication conditions used here (~23 kHz, 3 mm diameter ultrasonic tip), the acoustic pressure amplitude is greatest at the faceplate of the horn and decreases as the distance from the horn increases.[18] The addition of an electrode below the horn does not perturb the direct driving sound field as the value of *ka* is relatively low (0.098, see Figure 6). Hence, this clearly cannot explain the results reported here or the material effects observed. However, it is known that shock waves can be generated through cluster collapse events.[39−41] Evidence for the production of shock waves is given in an accompanying paper.[18] These shock waves, owing to their high frequency components (and hence high *ka* values), will be scattered from the surface of the electrode to a greater or lesser extent depending on the materials employed in the electrode construction (see Table 1). Hence, it is proposed that it is these shock waves that are responsible for the perturbation of the inertial cavitation threshold (as measured by both MBSL imaging and electrochemical erosion/corrosion measurements). In these cases, the enhanced distance effects observed are as a direct result of the invasive nature of the electrode employed within the sound field.

Discussion. The results reported in this paper emphasize the importance of considering the sound field and, in particular, the local acoustic pressure amplitude when analyzing and interpreting sonoelectrochemical results. Consider a bubble at a distance of 2 mm from the faceplate of the horn. In the presence of an epoxy electrode,[20] the acoustic pressure amplitude could be less than the inertial cavitation threshold (as measured in this work and elsewhere[18]) and no inertial (transient) cavitation effects would be observed. In contrast, if the electrode was constructed from glass (as employed extensively by Birkin et al.[15]), the local pressure amplitude may be greater due to a higher *R* value and more efficient reflection of any shock waves generated through the cavitation process. Under these conditions, inertial collapse is expected with the associated physical phenomena (such as surface erosion, large single mass transfer events[16,19] and MBSL). It is also interesting to note that as the size or nature of the electrode support is changed, the results will be altered. If the electrode support is increased in size (e.g., to $a \sim 2$ cm), then the direct sound field (23 kHz) will be effectively scattered and must also be considered.

Last, Figure 5 and Table 1 show that these differences in the invasive nature of the electrode within the sound field are most pronounced for epoxy (or materials with similar acoustic impedances, for example, PTFE) compared to glass or metals.

Conclusions

A dual electrode constructed in glass has been produced and a recessing method developed to produce a Pb/Pt combination. The effect of the glass support has been compared to a dual electrode produced within an epoxy based substrate. The scattering due to an electrode inserted into the sound field developed by an operating ultrasonic horn has been considered. The effects on the sound field, and hence the local pressure amplitude, have been investigated using MBSL and electrochemical experimental techniques. The invasive nature of electrodes within a cavitation plume has been demonstrated, and it is suggested that shock wave emission from cavity collapse processes significantly alters the results observed. The extent of the perturbation of the sound field by the electrode support has been quantified by acoustic impedance measurements of the relevant materials and solutions. The inertial threshold under the conditions employed here has been shown to occur at an axial distance of 1.3 ± 0.2 mm for epoxy and 2.3 ± 0.2 mm for glass supported electrodes.

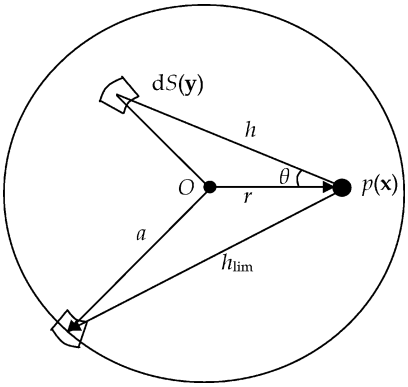

Figure 10. Diagram indicating the geometry considered on the surface of the disk (electrode substrate) with the various parameters employed in the analysis of the problem.

Acknowledgment. We thank the EPSRC for funding a studentship for D.G.O. under research grant GR/N30989/01.

Appendix

This appendix presents a theoretical investigation into the scattered pressure as a function of the radial distance across the electrode surface and the average pressure over the face of the electrode. By making the simplifying assumption that the axial particle velocity in the plane of the disk for $r > a$ is zero, where a is the disk radius and r the radial distance from the center of the electrode, Rayleigh's second integral can be applied to compute the scattered acoustic pressure at any position, $\mathbf{x}$, in space, including points on the disk surface. For a time-harmonic axial velocity distribution, u_s, of frequency ω, uniformly distributed over the disk surface, S, the scattered pressure may be written as

$$p_s(\mathbf{x},t) = \frac{-jk\rho_1 c_1 u_s e^{j\omega t}}{2\pi}\int_S \frac{e^{-jk|\mathbf{x}-\mathbf{y}|}}{|\mathbf{x}-\mathbf{y}|}\,\mathrm{d}S(\mathbf{y}) \qquad \text{(A1)}$$

where k is the acoustic wavenumber ($k = \omega/c_1$). Equation A1, together with the construction shown in Figure 10, gives the radial pressure distribution on the disk surface due to scattering of the incident pressure in the form

$$p_s(r,t) = \frac{-jkRp_i e^{j\omega t}}{2\pi}\int_{-\pi}^{\pi}\int_0^{h_{\lim}(r,\theta)} \frac{e^{-jkh}}{h} h\,\mathrm{d}h\,\mathrm{d}\theta \qquad \text{(A2)}$$

where from figure 10

$$h_{\lim}(r,\theta) = r\cos\theta + \sqrt{a^2 - r^2\sin^2\theta}$$

While the integral in h in eq A2 is straightforward, the integral over θ has no closed-form solution. The final result for the total acoustic pressure versus r may be written in the form shown in eq A3.

$$p(r,t) = p_i(t) + p_s(r,t) = p_i e^{j\omega t}[1 + R(1 - H(ka,\bar{r}))] \qquad \text{(A3)}$$

where $\bar{r} = r/a$ and $H(ka,\bar{r})$ is a scattering function given by

$$H(ka,\bar{r}) = \frac{1}{\pi}\int_0^{\pi}\exp[-j\Psi(\bar{r},\theta)]\,\mathrm{d}\theta$$

$$\Psi = ka(\bar{r}\cos\theta + \sqrt{1 - \bar{r}^2\sin^2\theta}) \qquad \text{(A4)}$$

Note that eq A4 indicates that the total pressure variation is completely defined by two nondimensional quantities: the (Helmholtz) frequency, ka, and the fractional radial distance, $\bar{r}$, from the center. The latter follows from the axisymmetry of the problem. Since the maximum value of $|H|$ equals unity, and considering a perfectly reflecting electrode, $R = 1$, eqs A3 and A4 reveal the following limiting behaviors for the mean square total pressure at the face of the electrode:

$$\overline{p^2}(r) \to \overline{p_i^2}[5 - 4\cos ka]; \quad r/a \to 0$$

$$\overline{p^2}(r) \to \overline{p_i^2}; \quad \text{for all } r \text{ as } ka \to 0$$

$$\overline{p^2}(r) \to 4\overline{p_i^2}; \quad \text{for all } r \text{ as } ka \to \infty \text{ (except } r = 0)$$

where $\overline{p_i^2} = (1/2)|p_i|^2$ is the mean square pressure of the incident sound field in the absence of the electrode. The general behavior of $\overline{p^2}(\bar{r})/\overline{p_i^2}$ versus $\bar{r}$ for a perfectly rigid electrode, $R = 1$, is plotted in Figure 11 for various ka values. Note that the value of $\overline{p^2}(\bar{r})/\overline{p_i^2}$ can be up to 9 times greater than in the absence of the electrode. To assess the average effect of the electrode on the sound field, we now consider the pressure averaged over the face of the electrode, defined by

$$\langle p\rangle = S^{-1}\int_S p(\mathbf{x})\,\mathrm{d}S(\mathbf{x}) \qquad \text{(A5)}$$

Substituting eqs A3 and A4 into eq A5 yields

$$\langle p\rangle = p_i e^{j\omega t}\left[1 + R\left(1 - \frac{2}{\pi}\int_0^{\pi}\int_0^1 \exp[-j\Psi(\bar{r},\theta)]\,\mathrm{d}\theta\bar{r}\,\mathrm{d}\bar{r}\right)\right] \qquad \text{(A6)}$$

Equation A6 is a numerical solution to the problem described by the analytical equation[42] in the main text (see eq 4). Comparing the surface averaged pressure predicted by eqs 4 and A6 (not shown) indicates excellent agreement between the two approaches.

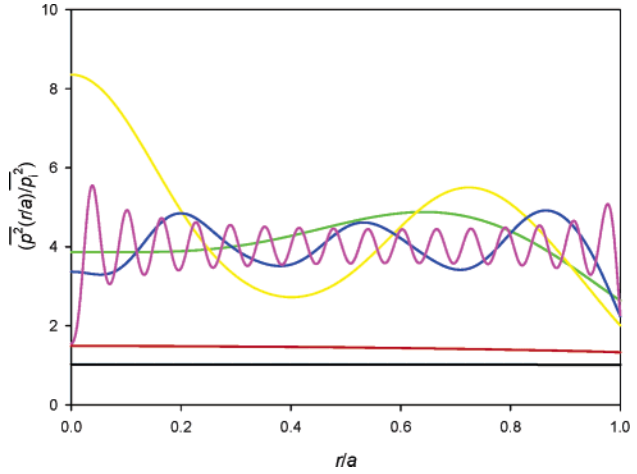

Figure 11. Plot showing the variation in the mean square scattered pressure normalized to the mean square incident pressure across the electrode surface as ka is varied. The black, red, green, yellow, blue, and magenta lines represent ka = 0.1, 0.5, 5, 10, 20, and 100, respectively.

References and Notes

(1) Moriguchi, N. *J. Chem. Soc. Jpn.* **1934**, *55*, 749.
(2) Moriguchi, N. *J. Chem. Soc. Jpn.* **1934**, *55*, 751.
(3) Rowe, W. E.; Nyborg, W. L. *J. Acoust. Soc. Am.* **1966**, *39*, 965.

(4) Nyborg, W. L.; Seegall, M. I. L. Effects of acoustic microstreaming at electrodes. Proceedings of the 3rd International Congress on Acoustics, 1960.

(5) Zhang, H. H.; Coury, L. A. *Anal. Chem.* **1993**, *65*, 1552.

(6) Walton, D. J. *Arkivoc* **2002**, *iii*, 198.

(7) Compton, R. G.; Eklund, J. C.; Marken, F.; Rebbitt, T. O.; Akkermans, R. P.; Waller, D. N. *Electrochim.* Acta **1997**, *42*, 2919.

(8) Klima, J.; Bernard, C.; Degrand, C. *J. Electroanal. Chem.* **1994**, *367*, 297.

(9) Hagan, C. R. S.; Coury, L. A. *Anal. Chem.* **1994**, *66*, 399.

(10) Marken, F.; Eklund, J. C.; Compton, R. G. *J. Electroanal. Chem.* **1995**, *395*, 335.

(11) Eklund, J. C.; Walker, D. N.; Rebbitt, T. O.; Marken, F.; Compton, R. C. *J. Chem. Soc., Perkin Trans.* **1995**, 1981.

(12) Compton, R. G.; Eklund, J. C.; Page, S. D. *J. Phys. Chem.* **1995**, *99*, 4211.

(13) Walton, D. J.; Phull, S. S.; Bates, D. M.; Lorimer, J. P.; Mason, T. J. *Electrochim. Acta* **1993**, *38*, 307.

(14) Birkin, P. R.; Silva-Martinez, S. *J. Chem. Soc., Chem. Commun.* **1995**, 1807.

(15) Birkin, P. R.; Silva-Martinez, S. *J. Electroanal. Chem.* **1996**, *416*, 127.

(16) Birkin, P. R.; Silva-Martinez, S. *Ultrason. Sonochem.* **1997**, *4*, 121.

(17) Birkin, P. R.; O'Connor, R.; Rapple, C.; Silva-Martinez, S. *J. Chem. Soc., Faraday Trans.* **1998**, *94*, 3365.

(18) Birkin, P. R.; Offin, D. G.; Leighton, T. G. *Phys. Chem. Chem. Phys.* **2005**, *7*, 530.

(19) Birkin, P. R.; Offin, D. G.; Leighton, T. G. *Electrochem. Commun.* **2004**, *6*, 1174.

(20) Maisonhaute, E.; White, P. C.; Compton, R. G. *J. Phys. Chem. B* **2001**, *105*, 12087.

(21) Birkin, P. R.; Leighton, T. G.; Power, J. F.; Simpson, M. D.; Vinçotte, A. M. L.; Joseph, P. F. *J. Phys. Chem. A* **2003**, *107*, 306.

(22) Leighton, T. G. *The Acoustic Bubble*; Academic Press: London, 1994.

(23) Gaitan, D. F.; Crum, L. A.; Church, C. C.; Roy, R. A. *J. Acoust. Soc. Am.* **1992**, *91*, 3166.

(24) Weissler, A.; Cooper, H. W.; Snyder, S. *J. Am. Chem. Soc.* **1950**, *72*, 1769.

(25) Weissler, A. *J. Am. Chem. Soc.* **1959**, *81*, 1077.

(26) Birkin, P. R.; Power, J. F.; Leighton, T. G. *J. Chem. Soc., Chem. Commun.* **2001**, 2230.

(27) Birkin, P. R.; Power, J. F.; Leighton, T. G.; Vinçotte, A. M. L. *Anal. Chem.* **2002**, *74*, 2584.

(28) Galloway, W. J. *J. Acoust. Soc. Am.* **1954**, *26*, 849.

(29) Saez, V.; Frias-Ferrer, A.; Iniesta, J.; Gonzalez-Garcia, J.; Aldaz, A.; Riera, E. *Ultrason. Sonochem.* **2005**, *12*, 59.

(30) Nyborg, W. L. Physical principles of ultrasound. In *Ultrasound; its applications in medicine and biology*; Fry, F. J., Ed.; Elsevier: New York, 1978.

(31) *CRC Handbook of Chemistry and Physics 1913−1995*, 75th ed.; CRC Press: 1995.

(32) Kaye, G. W. C.; Laby, T. H. *Tables of Physical and Chemical Constants and some Mathematical Functions*, 12th ed.; Longmans, Green and Co: London, 1959.

(33) www.goodfellow.com.

(34) Note the hydrophone (B&K 8103) used to measure the acoustic signature of the sound field produced (see ref 18) has an upper frequency limit of ∼180 kHz. Hence, it is unlikely to resolve the true frequency characteristics of the shocks produced by the cavitation process. However, Figure 4 of ref 18 shows these shock waves have a significantly raised frequency and higher amplitude (∼10 times the drive signal) when compared to the 23 kHz drive signal.

(35) Kinsler, L. E.; Frey, A. R.; Coppens, A. B.; Sanders, J. V. *Fundamentals of Acoustics*; John Wiley & Sons: New York, 1982.

(36) Leighton, T. G. *The Acoustic Bubble, section 2.1.2 and 4.3.1*; Academic Press: London, 1994.

(37) Berthelot, M. *Ann. Chim. Phys.* **1850**, *30*, 232.

(38) Green, J. L.; Durben, D. J.; Wolf, G. H.; Angell, C. A. *Science* **1990**, *249*, 649.

(39) Hansson, I.; Mørch, K. A. *J. Appl. Phys.* **1980**, *51*, 4651.

(40) Vyas, B.; Preece, C. M. *J. Appl. Phys.* **1976**, *47*, 5133.

(41) Hansson, I.; Kedrinskii, V.; Mørch, K. A. *J. Phys. D: Appl. Phys.* **1982**, *15*, 1725.

(42) Rayleigh, L. *Theory of Sound*, 2nd ed.; Macmillan: London, 1896.